Interface-related switching behaviors of amorphous $Pr_{0.67}Sr_{0.33}MnO_3$-based memory cells*

Zhang Ting(张 婷), Bai Ying(白 莹), Jia Cai-Hong(贾彩虹), and Zhang Wei-Feng(张伟风)†

Key Laboratory of Photovoltaic Techniques of Henan Province, School of Physics and Electronics, Henan University, Kaifeng 475004, *China*

(Received 17 February 2012; revised manuscript received 9 March 2012)

The resistive switching properties in amorphous $Pr_{0.67}Sr_{0.33}MnO_3$ films deposited by pulsed laser deposition are investigated. Reproducible and bipolar counter-8-shape and 8-shape switching behaviours of $Au/Pr_{0.67}Sr_{0.33}MnO_3/F{:}SnO_2$ junctions are obtained at room temperature. Dramatically, the coexistence of two switching polarities could be reversibly adjusted by an applied voltage range. The results allocated those two switching types to areas of different defect densities beneath the same electrode. The migration of oxygen vacancies and the trapping effect of electrons under an applied electric field play an important role. An interface-effect-related resistance switching is proposed in an amorphous $Pr_{0.67}Sr_{0.33}MnO_3$-based memory cell.

Keywords: $Pr_{0.67}Sr_{0.33}MnO_3$ thin films, resistance switching, amorphous, metal–oxide interface

PACS: 73.40.–c, 73.40.Rw, 73.50.Fq, 72.20.–i **DOI:** 10.1088/1674-1056/21/10/107304

1. Introduction

Resistive switching phenomena in metal–oxide-metal sandwich junctions, so-called "resistance random access memory (ReRAM)" and/or "memristors", have aroused a great deal of scientific and industrial interest as the next-generation of high-density non-volatile memory, owing to their structural simplicity and excellent characteristics compared with existing non-volatile memory such as flash-memory, magnetoresistive random access memory (MRAM), ferroelectric random access memory (FeRAM), and phase change random access memory (PRAM).[1−3] In 2000, Liu *et al.*[4] reported that $Pa_{0.7}Ca_{0.3}MnO_3/YBa_2Cu_3O_{7-\sigma}$ heterojunctions with Ag electrodes exhibited reversible switching by applying short voltage pulses. Since then, numerous perovskite-type transition-metal oxides, especially manganites,[5] titanates,[6,7] and zirconates[8] have been investigated as switching devices. In order to develop resistive materials applicable to memory cells and to reduce the ultimate scaling limits for future ReRAM, a deep understanding of the switching mechanism is indispensable. In recent years, some work has focused on amorphous binary oxide films such as HfO_2,[9] TiO_2,[10] Lu_2O_3,[11] and NbO_x,[12] which have already been proven to be compatible with CMOS technology. Moreover, without the limits of grain size and boundaries, devices using homogeneous amorphous films can be fabricated in a smaller area, to meet the demand of developing microelectronics. Furthermore, it is of pivotal importance to provide us with a new insight into the switching mechanism. However, there are few reports about resistive switching behaviours of ternary amorphous perovskite-type transition-metal oxides, and the intrinsic switching mechanism in the devices has not been clear up until now.

In the present work, we fabricate amorphous $Pr_{0.67}Sr_{0.33}MnO_3$ films by pulsed laser deposition (PLD) technology. The bipolar resistive switching properties of the amorphous PSMO films are observed, and a model based on the redistribution of the oxygen vacancy-related defects is suggested to explain their switching behaviours. Therefore, this study will lead to a better understanding of a perovskite-based memory device for non-volatile memory applications.

*Project supported by the National Natural Science Foundation of China (Grant No. 60976016), the Program for Innovative Research Team in Science and Technology in University of Henan Province (IRTSTUHN), China (Grant No. 2012IRTSTHN004), and the Foundation Co-established by the Province and the Ministry in Henan University, China (Grant No. SBGJ090503).

†Corresponding author. E-mail: wfzhang@henu.edu.cn

© 2012 Chinese Physical Society and IOP Publishing Ltd

2. Experimental details

The ceramic targets for PSMO were prepared by a standard solid state reaction method using $SrCO_3$, Pr_2O_3, and MnO_2 as the raw materials. The heterojunctions were fabricated by the PLD technique. PSMO thin films were grown on fluorine-doped tin oxide (FTO), conducting glass substrates at 600 °C using a KrF excimer laser ($\lambda = 248$ nm) with a repetition rate of 5 Hz and a single pulse power of 300 mJ. The deposition was carried out in a pure oxygen atmosphere at a pressure of 10 Pa. The morphologies of PSMO films were obtained with a JSM-5600 scanning electron microscope (SEM) and a SPA-400 atomic force microscope (AFM). The XRD patterns of the PSMO thin films were collected on a DX-2500 X-ray diffractometer, employing Cu Kα radiation (1.542 Å, 1 Å=0.1 nm). After deposition, a 20-nm thick circular Au electrode with an area of 7.1×10^{-4} cm^2 was patterned through a metal mask to form a sandwich structure by DC sputtering.

3. Results and discussion

In Fig. 1(a), the thickness of the deposition on the PSMO film is observed to be approximately 300 nm by SEM. The surface morphology of the deposition film is presented in Fig. 1(b). The 600-°C substrate temperature leads to quite a rough film surface. Tiny islands and sand pits with diameters ranging from 0.1 μm to 3 μm can be found. From Fig. 1(c), the XRD study shows no peak corresponding to PSMO diffraction except SnO_2 (FTO substrate) diffraction, indicating the films were amorphous.

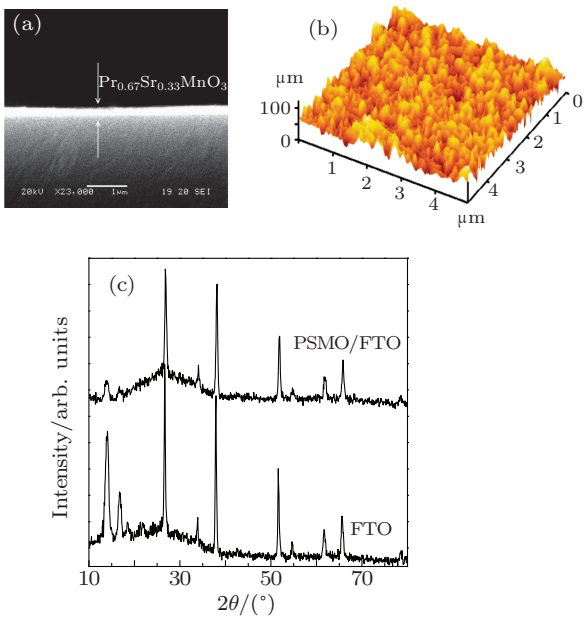


Fig. 1. (colour online) (a) Cross-section SEM images of the PSMO/FTO conducting glass structure. (b) AFM and (c) XRD patterns of the 300-nm-thick $Pr_{0.67}Sr_{0.33}MnO_3$ film deposited on the F:SnO_2 conducting glass substrate after annealing at 600 °C.

In order to gain an insight into the dynamic mechanism of charge carriers in the heterojunctions, the electrical measurements of switching were performed perpendicularly across the PSMO layer, using a current–voltage source meter (Keithly 2400) at room temperature and under ambient pressure. The F:SnO_2 film is used as the bottom electrode and the Au stack as the top electrode, with a small mechanical load applied. The data were obtained using a computer controlled program. A schematic drawing of the measurement configuration is depicted in the left-hand inset of Fig. 2.

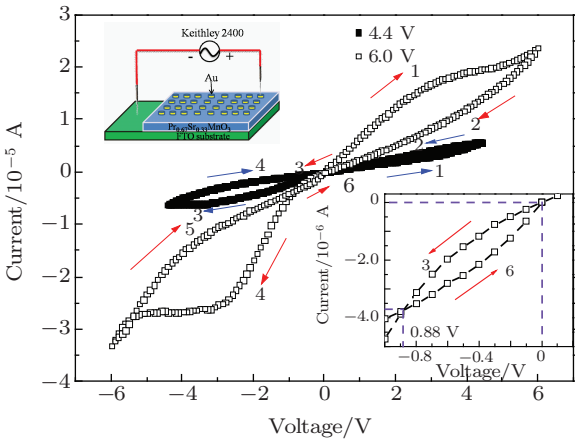


Fig. 2. (colour online) The I–V curves of the junction with an amorphous $Pr_{0.67}Sr_{0.33}MnO_3$ layer in different voltage regions. The left-hand inset presents the schematic plot of the measurement configuration, and the right-hand inset indicates the two crossing behaviour of I–V curves with 6.0-V sweeping voltage.

The current–voltage (I–V) characteristics are presented in Fig. 2. The I–V curves are obtained by continuously sweeping the voltage from 0 to V_{max} to 0 to $-V_{max}$ to 0, where V_{max} is the maximum of the applied bias voltage. One can see two types of switching properties represented by the open square and the solid square curves. The solid square curves are observed to be in a smaller voltage range of ±4.4 V. Starting at 0 V and sweeping to 4.4 V, the sample resides in branch "1". In the subsequent sweep, the voltage is swept back from 4.4 V to 0 V, and the sample switches into a low resistance state (branch "2"). Going up to –4.4 V and then back to 0 V again completes the switching cycle. In the following we call the

"sense of rotation" or the switching polarity of this curve the 8-shape polarity. When the bias increases from ±4.4 V to 6.0 V, however, a second type of stable switching can be achieved. The differential resistances start to appear and then the switching polarity is converted into the other direction counter-8-shape polarity (open square curve in Fig. 2). As the voltage sweeps from 0 V to 6 V to 0 V, the sample switches from a low resistance state to a high resistance state. Going back to negative voltages reverses this switching again. Both types of switchings occur in the same pad. A repeatable change between both curves can be induced by adjusting the voltage amplitude back and forth again.

From the *I*–*V* curve, the measured resistance value is much larger than that of polycrystalline ceramic (0.01 Ω·cm ∼ 0.2 Ω·cm). This deviation reminds us of the effect of the electrode/film interface. In the Au/PSMO/FTO heterostructure, the lower thermal energy during the deposition results in a local nonstoichiometry and thereby leading to a high density of defects in the PSMO layer. A high resistive region containing a high density of defects exists at the Au/PSMO interface, where the high density of surface states induced by the defects may cause a large degree of band bending thus influencing the validity of the metal/semiconductor contact rule. The dense interface defects act as trap centres of carriers and dominate the *I*–*V* characteristics and electric-pulse-induced resistance (EPIR) change properties. Up to date, similar interface-related electrical characteristics have been observed in many studies. Sawa *et al.*[13] believed that the resistance switching occurs only at the Ti/$Pr_{0.7}Ca_{0.3}MnO_3$ interface after investigating the effects of several top electrodes such as SRO, Pt, Au, Ag, and Ti on the resistance switching. Oka and Nagaosa[14] proposed a unique mechanism with a first order interface metal–insulator transition. Janousch *et al.*[15] pointed out that the microscopic origin of resistance switching in transition-metal–oxide-based memory is an oxygen–vacancy drift occurring in a place close to one of the electrodes. Recent studies have indicated that the electrochemical migration of oxygen vacancies in the vicinity of the interface drives resistive switching.[16−18] There exists a general agreement in oxides that the migration of oxygen vacancies (or oxygen ions) under an applied electric field plays an important role and that the interface effects are more pronounced than bulk switching. Two basic models have been proposed: (i) a local redox process based on oxygen vacancy migration (or oxygen diffusion)[19] including an electrochemical interface reaction[20] and (ii) a change in the Schottky-like barrier height and/or width by trapping/detrapping effects in interface defect states.[13] Although no attention has been paid to them in the literature yet, these two mechanisms exhibit different switching polarities. In p-type materials, the former changes resistance from a high resistance state (HRS) to a low resistance state (LRS) in the positive voltage polarity of the active electrode. The latter converts an LRS into an HRS under the same bias polarity. The same polarity changes occur in the negative bias in the case of n-type layers.[6]

For a better understanding of the influence of defects on the electric properties of the PSMO sample, XPS profiles are performed for the O 1s and Mn 2p regions. As can be seen in Fig. 3(a), the peaks are attributed to the existence of Mn^{4+} and Mn^{3+}, respectively. Such mixed oxides are naturally imperfect in their microstructure. In Fig. 3(b), the peaks in the O 1s spectra correlated with lattice oxygen bonding in PSMO at 529.1 eV and absorbed oxygen at 530.9 eV and 531.9 eV are observed at the PSMO surface. Dong *et al.*[21] reported that the absorbed oxygen could act as mobile oxygen and generate oxygen vacancies under a high electric field.[21] It is well known that in perovskite oxide, the ionization of the oxygen vacancies will create the conducting electrons,

$$\mathrm{O_O} \Leftrightarrow \mathrm{V_O} + 1/2\mathrm{O_2}, \tag{1}$$

$$\mathrm{V_O} \Leftrightarrow \mathrm{V_{\dot{O}}} + \mathrm{e}', \tag{2}$$

$$\mathrm{V_{\dot{O}}} \Leftrightarrow \mathrm{V_{\ddot{O}}} + \mathrm{e}', \tag{3}$$

or these electrons might be bonded to Mn^{4+} in the form of

$$\mathrm{Mn^{4+}} + e' \Leftrightarrow \mathrm{Mn^{3+}}. \tag{4}$$

Here, the notations defined by Kröger and Vink are adopted; $\mathrm{V_{\dot{O}}}$ and $\mathrm{V_{\ddot{O}}}$ represent the oxygen vacancies carrying one and two positive charges, respectively.[22] Oxygen vacancies create deep-trap energy levels in the band gap for activated electrons to be movable. The metallic ions or oxygen vacancies are very likely to exist in the matrix. Those defects are thought to play an important role in resistance hysteresis.

As is well known, PSMO is a p-type semiconductor that forms the basic element for resistance switching. In Fig. 2, the solid square curve switching with 8-shape polarity can be explained by oxygen–vacancy migration,[23,24] judging from the resistance

changes from HRS to LRS in the positive or the forward bias. This behaviour can be explained by considering the number of oxygen vacancies. In p-type oxide semiconductors, oxygen vacancies are considered to be an acceptor scavenger. The schematics of the relations between the oxygen vacancy density and the depletion layer width (W_d) in the vicinity of the Au/PSMO interface in different resistance states could be clearly seen in Fig. 4. A positive (negative) voltage rejects (accumulates) oxygen vacancies at the Au/PSMO interface. The reduction (addition) in oxygen vacancies at the interfaces may cause the depletion layer to become narrower (wider) in PCMO, resulting in a decrease (increase) in the contact resistance. For the oxygen-diffusion-related switching mechanism, extended defects within the active thin film matrix have been claimed to play a crucial role.[16,20,25] This is associated with the fact that oxygen–vacancy migration (or oxygen diffusion) is significantly enhanced along extended defects.[26] Shibuya *et al.*[6] demonstrated the clear correlation between resistive switching property and the density of defects which work as fast migration paths for oxygen vacancies in Au/Sr_2TiO_4/Nb-doped $SrTiO_3$ junctions. So we can induce that the 8-shape polarity is due to the oxygen–vacancy migration along the extended defects.

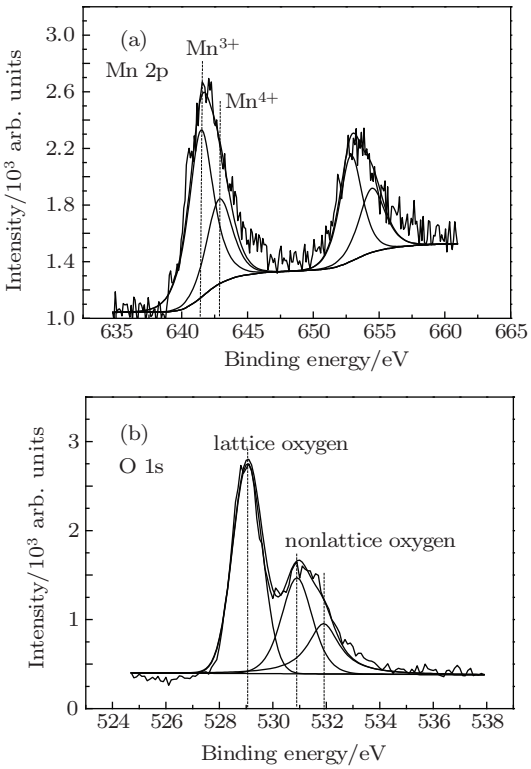


Fig. 3. XPS profiles for the (a) Mn 2p and (b) O 1s regions.

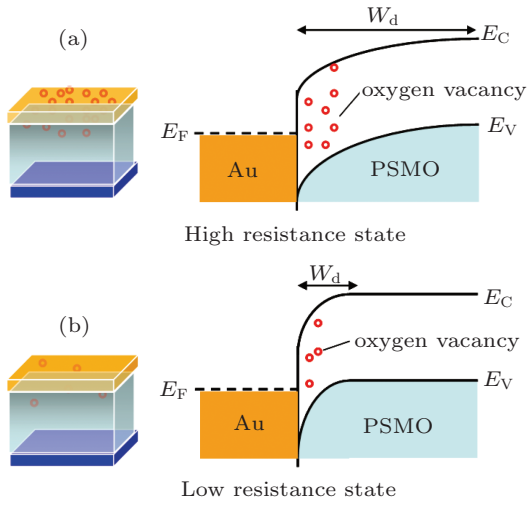


Fig. 4. (colour online) Schematics of the relationship between the oxygen–vacancy density and the depletion layer width (W_d) in the vicinity of the Au/PSMO interface at a high resistance state (a) and a low resistance state (b).

Due to the different work function values of Au (∼ 5.1 eV), FTO (∼ 4.4 eV),[27] and PSMO (∼ 4.9 eV),[28] the hole barriers should be formed at the Au/PSMO interface. The Schottky-like barrier height and/or width will be changed by trapping/detrapping effects at interface defect states. In Fig. 2, the other switching type (red curves) with "counter-8-shape polarity shows a rectification behaviour and I–V curves of the pristine junction. The Schottky-like barrier seems to be slightly modified during voltage sweeping. The enhancement of positive bias results in a reduction of the current. This behaviour can be attributed to the electron-trapping effect at the interface. When a large positive (negative) voltage is applied to the Schottky-like barrier, electrons are charged (discharged) in the trapping states, resulting in the reduction (addition) of the net positive (negative) charge in the depletion region. This makes the barrier wider (narrower) and higher (lower), which results in the HRS (LRS). So interface defects will dominantly influence the trapping/detrapping-based switching mechanism.

It is more interesting that the polarity conversion of these two switching types can be reversibly adjusted by the sweeping voltage range, as shown in Fig. 2. The HRS of the counter-8-shape polarity corresponds to the LRS of the 8-shape. The other major discovery is that the second intersection of the I–V curve exists in a large negative voltage range (open square curves). The right-hand inset of Fig. 2 clearly indicates the behavior of the two intersection points of the I–V curve with a 6.0-V sweeping voltage. The conversion of HRS and LRS emerges at about 0.88 V, where

the effect of oxygen–vacancy migration overcomes that of electron trapping. Therefore, the switching polarity is selective to the voltage range. This procedure might extract trapped oxygen vacancies from the interface. The pinning of oxygen vacancies at the interface may cause the depletion layer to become narrower and LRS to appear.

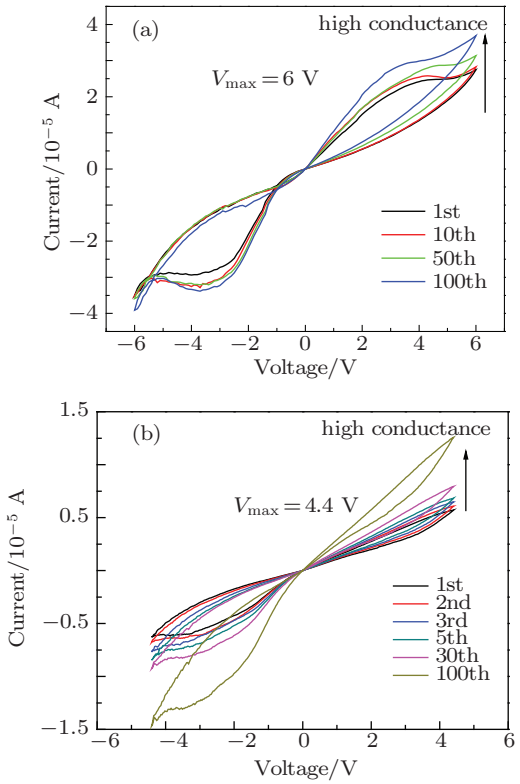


Fig. 5. (colour online) I–V curves obtained by multiple voltage sweeps, showing the changes (indicated by the arrows) from the first curves with lower conductance to the last curves with higher conductance in the case of (a) $V_{max} = 6.0$ V and (b) $V_{max} = 4.4$ V.

To investigate the changes in conductance as a function of sweeping cycle, an experiment is performed. Note that switching with 8-shape polarity seems to be more stable than the others. When sweeping the voltage over multiple cycles, a change can be observed in the I–V curves from the first to the following runs, i.e. a memory effect in the sample. In Fig. 5 the first I–V curve presents a lower conductance than all the later curves, while the last curve presents a higher conductance. In the framework of the model discussed above, the following interpretation is proposed. When the device is switched on from its virgin state, oxygen vacancies or electrons will reaccommodate at different positions. When the device is switched off, not all the ions will migrate back to their original positions, and the accumulation of oxygen vacancies or electrons at the negative electrode will not be completely undone. This supports the assumption that permanent changes occur in the sample when mass transport of ions appears. Statistical investigation on the exact nature of defects is essential for further understanding of resistive switching.

4. Conclusions

In the present paper, the well-developed bipolar resistive switching properties are revealed in amorphous PSMO heterojunctions. An interface-effects-related resistance switching is proposed in the memory cell. By reversibly adjusting the applied voltage range, the coexistence of two switching polarities could be observed repeatedly. The migration of oxygen vacancies and the trapping effect of electrons under an applied electric field play an important role. Up to now, switching polarities have been rarely discussed in the literature. It is suggested to allocate the two switching types to areas of different defect densities beneath the same electrode. Therefore, the control of the distribution and the density of defects is a major task in the fabrication of reproducible and scalable resistive switching devices. We believe that these are crucial points in understanding the switching mechanisms.

References

[1] Garcia V, Fusil S, Bouzehouane K, Enouz-Vedrenne S, Mathur N D, Barthélémy A and Bibes M 2009 *Nature* **460** 81
[2] Li Y T, Long S B, Lü H B, Liu Q, Wang Q, Wang Y, Zhang S, Lian W T, Liu S and Liu M 2011 *Chin. Phys.* B **20** 017305
[3] Zhang T, Ding L H and Zhang W F 2012 *Chin. Phys.* B **21** 047301
[4] Liu S Q, Wu N J and Ignatiev A 2000 *Appl. Phys. Lett.* **76** 2749
[5] Lee W, Jo G, Lee S, Park J, Jo M, Lee J, Jung S, Kim S, Shin J, Park S, Lee T and Hwang H 2011 *Appl. Phys. Lett.* **98** 032105
[6] Shibuya K, Dittmann R, Mi S and Waser R 2010 *Adv. Mater.* **22** 411
[7] Muenstermann R, Menke T, Dittmann R and Waser R 2010 *Adv. Mater.* **22** 4819
[8] Cho S, Park W G, Cho D Y, Berthet P and Oh S J 2010 *J. Appl. Phys.* **108** 103716
[9] Yu S, Gao B, Dai H B, Sun B, Liu L F, Liu X Y, Han R Q, Kang J F and Yu B 2010 *Solid-State Lett.* **13** H36
[10] Jeong H Y, Lee J Y and Choi S Y 2010 *Adv. Funct. Mater.* **20** 3912
[11] Gao X, Xia Y D, Xu B, Kong J Z, Guo H X, Li K, Li H T, Xu H N, Chen K, Yin J and Liu Z G 2010 *J. Appl. Phys.* **108** 074506
[12] Jung K, Kim Y, Jung W, Im H, Park B, Hong J, Lee J, Park J and Lee J K 2010 *Appl. Phys. Lett.* **97** 233509

[13] Sawa A, Fujii T, Kawasaki M and Tokura Y 2004 *Appl. Phys. Lett.* **85** 4073

[14] Oka T and Nagaosa N 2005 *Phys. Rev. Lett.* **95** 266403

[15] Janousch M, Meijer G I, Staub U, Delley B, Karg S F and Andreasson B P 2007 *Adv. Mater.* **19** 2232

[16] Tsui S, Baikalov A, Cmaidalka J, Sun Y Y, Wang Y Q, Xue Y Y, Chu C W, Chen L and Jacobson A J 2004 *Appl. Phys. Lett.* **85** 317

[17] Seong D, Jo M, Lee D and Hwang H 2007 *Solid-State Lett.* **10** H168

[18] Nian Y B, Strozier J, Wu N J, Chen X and Ignatiev A 2007 *Phys. Rev. Lett.* **98** 146403

[19] Baikalov A, Wang Y Q, Shen B, Lorenz B, Tsui S, Sun Y Y, Xue Y Y and Chu C W 2003 *Appl. Phys. Lett.* **83** 957

[20] Waser R, Dittmann R, Staikov G and Szot K 2009 *Adv. Mater.* **21** 2632

[21] Dong R, Xiang W F, Lee D S, Oh S J, Seong D J, Heo S H, Choi H J, Kwon M J, Chang M, Jo M, Hasan M and Hwang H 2007 *Appl. Phys. Lett.* **90** 182118

[22] Xia Y D, Liu Z G, Wang Y, Shi L, Chen L, Yin J and Meng X K 2007 *Appl. Phys. Lett.* **91** 102904

[23] Fujii T, Kawasaki M, Sawa A, Kawazoe Y, Akoh H and Tokura Y 2007 *Phys. Rev.* B **75** 165101

[24] Janousch M, Meijer G I, Staub U, Delley B, Karg S F and Andresson B P 2007 *Adv. Mater.* **19** 2232

[25] Yang J J, Pickett M D, Li X, Ohlberg D A A, Stewart D R and Williams R S 2008 *Nat. Nanotechnol.* **3** 429

[26] Szot K, Speier W, Carius R, Zastrow U and Beyer W 2002 *Phys. Rev. Lett.* **88** 075508

[27] Bernède J C, Cattin L, Morsli M and Berredjem Y 2008 *Sol. Energy Mater. Sol. Cells* **92** 1508

[28] Reagor D W, Lee S Y, Li Y and Jia Q X 2004 *J. Appl. Phys.* **95** 7971